TITLE: Direct Calculation of Cavity Noise and Validation of Acoustic Analogies

Direct Calculation of Cavity Noise and Validation of Acoustic Analogies

Xavier Gloerfelt, Christophe Bailly and Daniel Juvé

Laboratoire de Mécanique des Fluides et d'Acoustique
Ecole Centrale de Lyon & UMR CNRS 5509
BP 163, 69131 Ecully cedex, France.

1. Introduction

Flow-induced cavity noise is a harmful noise source in many applications.[1] A complex nonlinear phenomenon is responsible for the intense self-sustained oscillations observed in experiments. However, the pysics is difficult to model analytically. The tonal Strouhal numbers are well approximated by Rossiter's formula[2] for a wide range of configurations but this simple semi-empirical analysis is not able to indicate the main oscillation mode neither its amplitude. Moreover, it is now generally recognized that noise generation mechanism can be dependent on the incoming boundary layer, the geometric properties of the cavity, the Mach number of the mean flow, and many other parameters. To predict detailed assessments of noise generation in complex cases, direct evaluation from fluid mechanics equations through DNS or LES with CAA tools represents the most thorough technique currently available. Nevertheless, the storage requirement and computation time make simulations of both the flow and acoustic fields difficult for realistic applications.

An alternative approach for computing the cavity noise consists of a two step calculation: nonlinear generation of sound and linear sound propagation. Once sources have been identified, with CFD or CAA calculations, there are several techniques to calculate the resulting radiated field. In this work, we propose to study numerical issues of three integral formulations: the Ffowcs Williams and Hawkings (FW-H) analogy which extends Lighthill's theory to account for solid boundaries and two Wave Extrapolation Methods (WEM) from a control surface, the Kirchhoff and porous FW-H methods. All these integral formulations have similar analytical insights based on Green's function formalism and suffer from the limitation of the observer in a uniform flow. The linear wave equation is assumed valid outside the source region, so that nonlinear propagation of acoustic waves is also not described.

In the first part of this paper, we shall present the direct computation of Navier-Stokes equations for a two-dimensional rectangular cavity with aspect ratio of 2, matching one configuration of Karamcheti's experiments.[3] In the second part, the far-field noise, associated with sources computed from the previous DNS, is obtained using the three integral formulations. Each method shall

Paper presented at the RTO AVT Symposium on "Ageing Mechanisms and Control: Part A – Developments in Computational Aero- and Hydro-Acoustics", held in Manchester, UK, 8-11 October 2001, and published in RTO-MP-079(I).

be described and the results shall be compared with those of direct acoustic simulation taken as a reference.

2. Direct computation of cavity noise

2.1 Introduction

Despite the amount of numerical studies published on cavity flows, few deal with radiated noise. Initial attemps have been made in supersonic cases, where acoustic field is dominated by shock waves radiation. These CFD computations of compressible cavity flows used the two dimensional unsteady RANS (Reynolds Averaged Navier-Stokes) equations with a turbulence model.[4,5] The first computations of acoustic radiation from a cavity with a subsonic grazing flow have been carried out recently by Colonius *et al.*,[6] and Shieh & Morris[7] using 2-D Direct Numerical Simulation (DNS) at a Reynolds number based on cavity depth $\mathrm{Re}_D \simeq 5000$. To investigate higher Reynolds numbers ($\mathrm{Re}_D \simeq 2 \times 10^5$), Shieh & Morris[8] applied CAA tools to solve unsteady RANS with a turbulence model: the one equation Spalart-Allmaras turbulence model and Detached Eddy Simulation have been implemented.

In the present work, the tested configuration is a 2-D rectangular cavity with $L/D = 2$, where $L = 5.18$ mm is the cavity length and $D = 2.54$ mm is its depth. The incoming flow is a laminar boundary layer with a Mach number M= 0.7 and a thickness $\delta \approx 0.2D$. The Reynolds number chosen is $\mathrm{Re}_D = 41000$ in order to match Karamcheti's experiment.[3] The latter studied the acoustic radiation from two-dimensional rectangular cavities cut into a flat surface at low Reynolds numbers. The acoustic fields were investigated by means of Schlieren observations, interferometry, and hot-wire anemometer. In our simulation, the freestream air temperature T_∞ is 298.15 K and the static pressure p_∞ is taken as 1 atm. The relatively thick incoming boundary layer ensures the shear layer mode of oscillations.[9] The choice of a high subsonic speed is interesting because the frequency increases slightly with Mach number and the cavity is no more compact relatively to the acoustic wavelength. Moreover, the test case is more relevant for integral methods because mean flow effects on sound propagation are important.

2.2 Numerical procedure

A Direct Numerical Simulation (no turbulence model) of the 2-D compressible Navier-Stokes equations is performed. These governing equations are discretized with a fourth order, seven-point stencil, DRP differencing operator spatially, and are advanced in time with the use of an explicit 4th order Runge-Kutta scheme.[9,10] Nonreflecting conditions are implemented to avoid spurious reflections which can superpose to physical waves. To this end, the radiation boundary conditions of Tam and Dong,[11] using a polar asymptotic solution of the linearized Euler equations in the acoustic far-field, are applied to the inflow and upper boundaries. At the outflow, we combine the outflow boundary conditions of Tam and Dong, where the asymptotic solution is modified to allow

the exit of vortical and entropic disturbances, with a sponge zone to dissipate vortical structures in the region where the shear layer leaves the computational domain. This sponge zone uses grid stretching and progressive additional damping terms.[10] Along the solid walls, the nonslip condition applies. The wall temperature T_w is calculated using the adiabatic condition. We keep centered differencing at the wall to ensure sufficient robustness using ghost points.

The computational mesh is built up from nonuniform Cartesian grid with 147×161 points inside the cavity and 501×440 outside, highly clustered near the walls. The minimum step size corresponds to $\Delta y^+_{min} = 0.8$ in order to resolve the viscous sublayer. The computational domain extends over $8.5D$ vertically and $12D$ horizontally to include a portion of the radiated field. The upstream and downstream boundaries are sufficiently far away from the cavity to avoid possible self-forcing. The initial condition is a polynomial expression of the laminar Blasius boundary layer profile with no forcing terms. Owing to the strong anisotropic computational mesh, we have a very stiff discretized system. For explicit time marching schemes, an extremely small time step has to be used in order to satisfy the stability CFL criterion: $\Delta t = 0.7 \times \Delta y_{min}/c_\infty = 6.06 \times 10^{-9}$ s. A selective damping, with a mesh Reynolds number of $R_S = 4.5$, has to be introduced in order to filter out non physical short waves resulting from the use of finite differences and/or treatment of boundary conditions. It is applied a second time near the walls. The computation is 4 hours long on a Nec SX-5.

2.3 Results and discussion

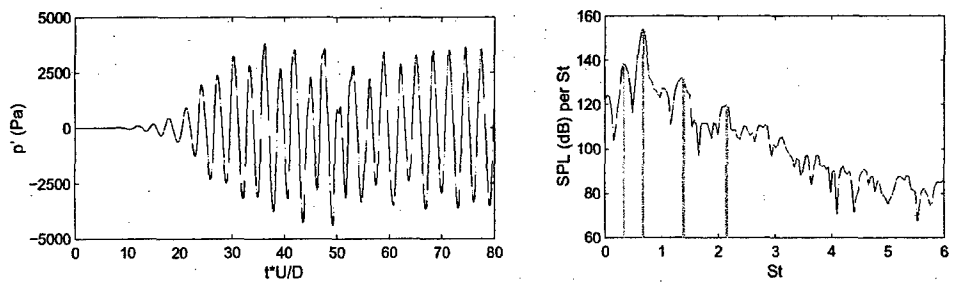

Figure 1: a) Pressure history versus time, and b) Spectrum of pressure fluctuations versus the Strouhal number $St = fL/U_\infty$, at $x/D = -0.04$ and $y/D = 2D$.

Figure 1a gives a monitored pressure history in the near-field acoustic region. The flow reaches a self-sustained oscillatory state after a time of about $25D/U_\infty$ but is still irregular until $65D/U_\infty$. This transient time corresponds with the time needed by the recirculating flow to get installed in the cavity. The associated sound pressure level spectrum is depicted in figure 1b, and displays one principal peak at St= 0.68. Several secondary peaks are noticeable and represent harmonics or subharmonics of the fundamental mode f_0. The experimental Strouhal number of oscillations is St= 0.71. This error of 5% on the predicted frequency can be explained by the different incoming

flow parameters or by the neglected 3-D effects.

A snapshot of vorticity depicted in figure 2a shows the presence of two vortical structures convected in the shear layer and impinging periodically the downstream edge of the cavity at the frequency f_0. The induced compression waves travel upstream and excite the shear layer at the separation point near the leading edge, sustaining the oscillation process. The Rossiter semi-empirical formula[2] provides St= 0.71 for this configuration with always two vortices in the shear layer.

A Schlieren visualization, corresponding with vertical gradients of density, shows the structure of the radiated field in figure 2b. Two wave patterns are visible for the positive gradients (dark), which interfer during propagation. Their strong upstream directivity is characteristic of high speed convection by the free stream. These radiations are in qualitatively good agreement with the Schlieren picture taken from Karamcheti's experiment. From finite-frange interferometry, Karamcheti[3] estimated an overall pressure level of about 160 dB at a distance of around three cavity depths. The spectrum of figure 1b indicates a level of 156 dB at $2.9D$.

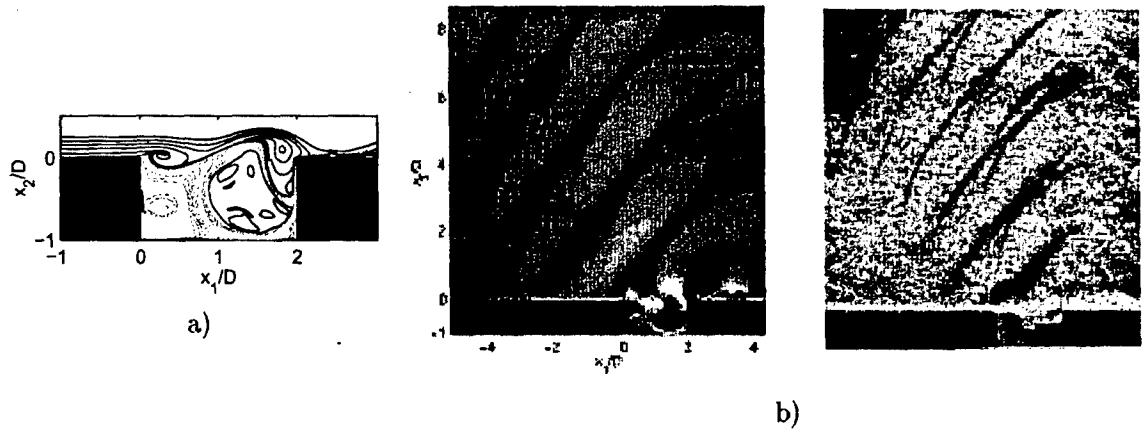

Figure 2: a) Snapshot of vorticity contours (16 contours between $\omega D/U_\infty =$ 10.5 and 1.36: (——) negative contours, (——) positive contours). b) Schlieren pictures corresponding to transversal derivative of the density: present simulation on the left, Karamcheti's experiment[3] on the right.

3. Validation of integral methods

Integral methods rest upon two principal physical backgrounds: first, the acoustic analogy which split the computational domain in an aerodynamic region, where source terms responsible for noise generation are built up, and an acoustic region governed by a linear wave equation; second, the wave extrapolations which allow the evaluation of the far-field once some quantities are known on a control surface.

Recent advances in integral methods were essentially developed for the reduction of helicopter rotor noise[12] and have been recently applied for the prediction of jet noise.[13,14] Zhang, Rona, and Lilley[5] have used Curle's spatial formulation to obtain far-field spectra of cavity noise.

3.1 Acoustic analogy

The acoustic analogy was proposed by Lighthill[15] and was extended by Ffowcs Williams and Hawkings[16] to include the effects of solid surfaces in arbitrary motion. The FW-H equation is an exact rearrangement of the continuity equation and Navier-Stokes equations into the form of an inhomogeneous wave equation with two surface source terms and a volume source term. An integral solution can thus be obtained by convoluting the wave equation with the free-space Green function.

A serious restriction is that the observation region is assumed at rest. It is difficult to extend the propagation operator to include more complex flows. Only the case of a uniform flow is satisfactorily treated. Ffowcs Williams and Hawkings proposed the use of a Lagrangian coordinate transform assuming the surface is moving in a fluid at rest. Goldstein[17] preferred to take the convection effects in the wave equation. In the same manner, in the case of a motion with constant velocity $\mathbf{U}_\infty = (U_1, 0)$, the application of the Galilean transformation from the observer position $(\tilde{\mathbf{x}}, t)$, moving at $-\mathbf{U}_\infty$ to the fixed location $(\mathbf{x}, t)$, defined by:

$$x_i = \tilde{x}_i + U_i t,$$

leads to the convected FW-H equation[18]:

$$\left(\frac{\partial^2}{\partial t^2} + U_i U_j \frac{\partial^2}{\partial x_i x_j} + 2U_i \frac{\partial^2}{\partial x_i t} - c_\infty^2 \frac{\partial^2}{\partial x_i^2}\right)\left(H(f) c_\infty^2 \rho'(\mathbf{x}, \omega)\right)$$
$$= \frac{\partial^2}{\partial x_i \partial x_j}\left(\tilde{T}_{ij}(\mathbf{x}, \omega) H(f)\right) - \frac{\partial}{\partial x_i}\left(\tilde{F}_i(\mathbf{x}, \omega)\delta(f)\right) + \frac{\partial}{\partial t}\left(\tilde{Q}(\mathbf{x}, \omega)\delta(f)\right) \quad (1)$$

where the modified source terms including convection can be written as:

$$\tilde{T}_{ij} = \rho(u_i - U_i)(u_j - U_j) + \left[p - c_\infty^2 \rho'\right]\delta_{ij} - \tau_{ij} \quad (2)$$

$$\tilde{F}_i = \left[\rho_\infty U_i U_j + p\delta_{ij} - \tau_{ij}\right]\frac{\partial f}{\partial x_j} \quad (3)$$

$$\tilde{Q} = \left[-\rho_\infty U_j\right]\frac{\partial f}{\partial x_j} \quad (4)$$

H is the Heaviside function and the function $f = 0$ defines the surface Σ outside of which the density field is calculated. f is scaled so that $\partial f / \partial x_j = n_j$, the j-component of the unit normal vector pointing toward the observer domain ($f > 0$). For a rigid body, we have simplified the surface source terms using the impenetrability condition $\mathbf{u}.\mathbf{n} = 0$.

For bidimensional geometries, it is more convenient to resolve this equation in the spectral-domain.[18] The frequency-domain formulation avoids the evaluation of the retarded time, which can be a critical point. The gain over the time-domain applications is enhanced in 2-D because of the weaker properties of the Heaviside function which replaces the Dirac function. Whereas the Dirac leads to a retarded time expression removing the temporal integration, the Heaviside function can

only change the upper limit of the integration to a finite value, the lower limit remaining infinite. The spectral formulation removes this time constraint by solving FW-H equation harmonically. With application of the Fourier transform:

$$\mathcal{F}\left[\phi(\mathbf{x},t)\right] = \phi(\mathbf{x},\omega) = \int_{-\infty}^{\infty} \phi(\mathbf{x},t) e^{-i\omega t}\, dt \tag{5}$$

equation (1) becomes

$$\begin{aligned}&\left(\frac{\partial^2}{\partial x_i^2} + k^2 - 2iM_i k\frac{\partial}{\partial x_i} - M_i M_j \frac{\partial^2}{\partial x_i \partial x_j}\right)\left(H(f)c_\infty^2 \rho'(\mathbf{x},\omega)\right)\\ &= -\frac{\partial^2}{\partial x_i \partial x_j}\left(\tilde{T}_{ij}(\mathbf{x},\omega)H(f)\right) + \frac{\partial}{\partial x_i}\left(\tilde{F}_i(\mathbf{x},\omega)\delta(f)\right) - i\omega\tilde{Q}(\mathbf{x},\omega)\delta(f)\end{aligned} \tag{6}$$

where $M_i = U_i/c_\infty$. A Green function for this inhomogeneous convected wave equation is obtained from a Prandtl-Glauert transformation of the 2-D free-space Green's fonction in the frequency domain:

$$G(\mathbf{x} \mid \mathbf{y},\omega) = \frac{i}{4\beta} e^{i(Mk(x_1-y_1)/\beta^2)} H_0^{(2)}\left(\frac{k}{\beta^2} r_\beta\right) \tag{7}$$

where $r_\beta = \sqrt{(x_1-y_1)^2 + \beta^2(x_2-y_2)^2}$, $H_0^{(2)}$ is the Hankel function of the second kind and order zero, and $\beta = \sqrt{1-M^2}$ is the Prandtl-Glauert factor, M< 1. The integral solution of equation (6) is then given by:

$$\begin{aligned}H(f)p'(\mathbf{x},\omega) = &-\int_{f=0} \tilde{F}_i(\mathbf{y},\omega)\frac{\partial G(\mathbf{x} \mid \mathbf{y})}{\partial y_i}\, d\Sigma - \int_{f=0} i\omega\tilde{Q}(\mathbf{y},\omega)G(\mathbf{x} \mid \mathbf{y})\, d\Sigma\\ &- \iint_{f>0} \tilde{T}_{ij}(\mathbf{y},\omega)\frac{\partial^2 G(\mathbf{x} \mid \mathbf{y})}{\partial y_i \partial y_j}\, d\mathbf{y}\end{aligned} \tag{8}$$

In 2-D, the volume integral is restricted to the surface including the aerodynamic sources T_{ij} and the surface integrals are calculated on the solid lines which represent rigid boundaries. We applied the spatial derivatives on the Green function to avoid the evaluation of derivatives of aerodynamic quantities. It is formally equivalent to the transformation in temporal derivatives as performed by di Francescantonio[19] or Farassat and Myers.[20]

3.2 Wave extrapolation methods

This kind of methods permits one to solve linear wave propagation problem once some flow quantities are given on a closed fictitious surface surrounding all the sources. The most famous one is the Kirchhoff method which makes a parallel with electromagnetism by using Kirchhoff's formula, published in 1883. The use of the FW-H equation for a permeable surface can provide an alternative extrapolation method as noted in the original Ffowcs Williams and Hawkings paper.[16] This method has been recently implemented by di Francescantonio.[19] At nearly the same time, Brentner and Farassat[21] demonstrated the relationship between the FW-H equation and the Kirchhoff equation for moving surfaces. The FW-H and Kirchhoff formulations solve the same physical problem, the differences between the two writings being due to some choices made in the derivation process.

The main advantage of wave extrapolation methods with respect to acoustic analogy approaches is that only surface integrals have to be evaluated because all non linear quadrupolar sources are enclosed in the control surface. The problem is thus reduced by one dimension, which is particularly interesting in a numerical point of view.

The convected Kirchhoff method

For a moving medium, the acoustic pressure at an arbitrary point $\mathbf{x}$ and time t is related to the distribution γ of sources within V and the distribution of the pressure and its derivative on the boundary of V by the generalized Green's formula.[17] For a 2-D configuration, it can be written as:

$$H(f)p'(\mathbf{x},t) = \int_{-\infty}^{\infty} \iint_{V(f>0)} \gamma(\mathbf{y},\tau) G(\mathbf{x},t|\mathbf{y},\tau)\, d\mathbf{y} d\tau + \int_{-\infty}^{\infty} \int_{\Sigma(f=0)} \left\{ G\frac{\partial p}{\partial y_i} - p\frac{\partial G}{\partial y_i} \right\} n_i\, d\Sigma(\mathbf{y}) d\tau + \frac{U_1}{c_\infty^2} \int_{-\infty}^{\infty} \int_{\Sigma(f=0)} \left\{ p\frac{DG}{D\tau} - G\frac{Dp}{D\tau} \right\} n_1\, d\Sigma(\mathbf{y}) d\tau$$

where D/Dt is the time rate of change seen by an observer moving along with the mean flow. Expressing the Green's function in the frequency-domain (7) and assuming all the quadrupolar source γ are included in Σ, we obtain:

$$H(f)p'(\mathbf{x},\omega) = \frac{i\beta}{4} \int_{f=0} \left\{ \frac{\partial p(\mathbf{y},\omega)}{\partial n_\beta} H_0^{(2)}\left(\frac{k}{\beta^2} r_\beta\right) + \frac{k}{\beta^2} p(\mathbf{y},\omega) \left[\frac{\partial r_\beta}{\partial n_\beta} H_1^{(2)}\left(\frac{k}{\beta^2} r_\beta\right) - i\mathrm{M}\frac{\partial y_1}{\partial n_\beta} H_0^{(2)}\left(\frac{k}{\beta^2} r_\beta\right) \right] \times \exp\left(i\frac{\mathrm{M}k(x_1 - y_1)}{\beta^2} \right) \right\} d\Sigma_\beta \qquad (9)$$

where n_β and $d\Sigma_\beta$ are the Prandtl-Glauert transforms of n and $d\Sigma$. This is the bidimensional Kirchhoff formulation for a uniformly moving medium in the frequency-domain.

The Ffowcs Williams and Hawkings WEM

This method is sometimes called the porous FW-H method because it coincides with the application of the FW-H analogy on a fictitious porous surface. The analytical developments are the same that those of the FW-H analogy but the impenetrability condition is no more required, and, on the contrary, one has to allow a fluid flow across Σ. For a two-dimensional problem with uniform subsonic motion, the FW-H WEM is given by equation (8) without the volume integral:

$$H(f)p'(\mathbf{x},\omega) = -\int_{f=0} \tilde{F}_i(\mathbf{y},\omega) \frac{\partial G(\mathbf{x} \mid \mathbf{y})}{\partial y_i}\, d\Sigma - \int_{f=0} i\omega \tilde{Q}(\mathbf{y},\omega) G(\mathbf{x} \mid \mathbf{y})\, d\Sigma \qquad (10)$$

with the two source terms:

$$\tilde{F}_i = [\rho(u_i - 2U_i)u_j + \rho_\infty U_i U_j + p\delta_{ij} - \tau_{ij}] \frac{\partial f}{\partial x_j} \qquad (11)$$

$$\tilde{Q} = [\rho u_j - \rho_\infty U_j] \frac{\partial f}{\partial x_j} \qquad (12)$$

3.3 Numerical implementation

From an algorithmic point of view, there is almost no difference between the three integral approaches considered here. The first step is the recording of the aerodynamic quantities during one period of the DNS computation. The acoustic time step is 40 times the DNS time step corresponding to 131 points per period. In the convected Kirchhoff method, the pressure distribution and its normal derivative over the three lines L_1, L_2, and L_3 spanning the longitudinal direction are needed to perform the surface integration. The normal derivative $\partial p/\partial y_2$ is not directly available from the near field solution and is here calculated with the DRP scheme. The variables (u_1, u_2, p, ρ) are recorded on the same three fictitious lines for the FW-H WEM, and on the walls of the cavity and the surface around it for the FW-H analogy application as reported in figure 3.

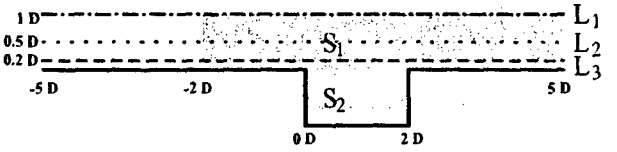

Figure 3: Schematic of the different line and surface sources for evaluation of integral formulations.

The source terms are calculated and transformed in the frequency-domain using the Fourier transform defined by (5). The integrals are then evaluated for each point of an acoustic meshgrid. This regular cartesian grid of 176 × 184 points covers a area of $(-5D; 5D) \times (-1D; 8D)$, corresponding with the main part of acoustic domain of DNS. Endly, an inverse Fourier transform is used to recover the acoustic signal in time-domain.

3.4 Results and discussions

In the Kirchhoff method, the results of the integration of (9) over L_1, L_2, and L_3 are depicted in figure 4. Same results are obtained for the extrapolation using the permeable form of the FW-H equation. The pressure fields from integration over L_1, L_2, and L_3 with source terms defined by (11), and (12), and with M= 0.7 in the observer domain are compared in figure 5. All the computed far-fields are consistent with that of DNS depicted in figure 6b, even when the control surface is located in the near-field region. The contour plots are only little sharper when the surface is farther from sources because more nonlinear effects are included in the control surface. In this configuration, the additional nonlinear terms appearing in the surface integrals of FW-H WEM but missing in the Kirchhoff formulation as noted by Brentner and Farassat[21] do not play a significant role and do not lead to the drastic differences observed in some previous comparisons when the control surface is too close to the sources.[21,22] Like di Francescantonio[19] or Prieur and Rahier,[23] we notice a similar behaviour of the two extrapolation methods. The advantage of porous FW-H method is only the fact that it uses directly the quantities computed by direct simulation without the need of further numerical process.

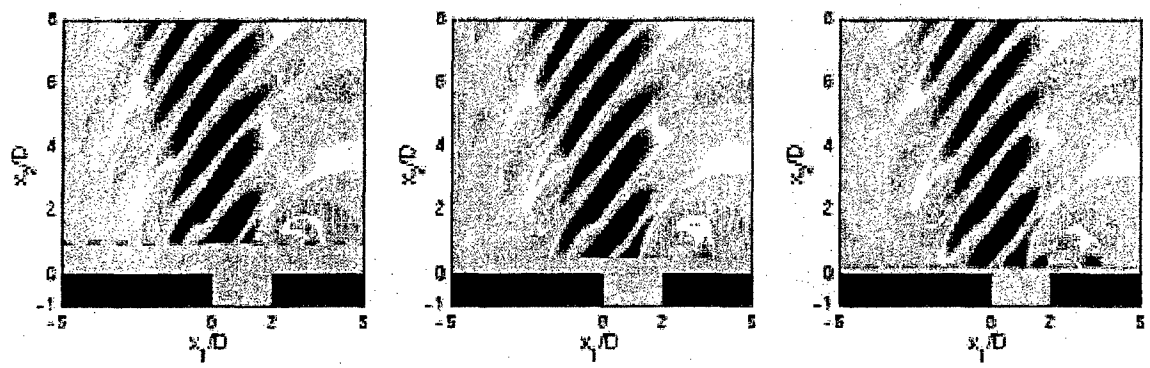

Figure 4: Pressure field ealculated at the same time by a) Kirchhoff's method from L_1, b) Kirchhoff's method from L_2, c) Kirchhoff's method from L_3.

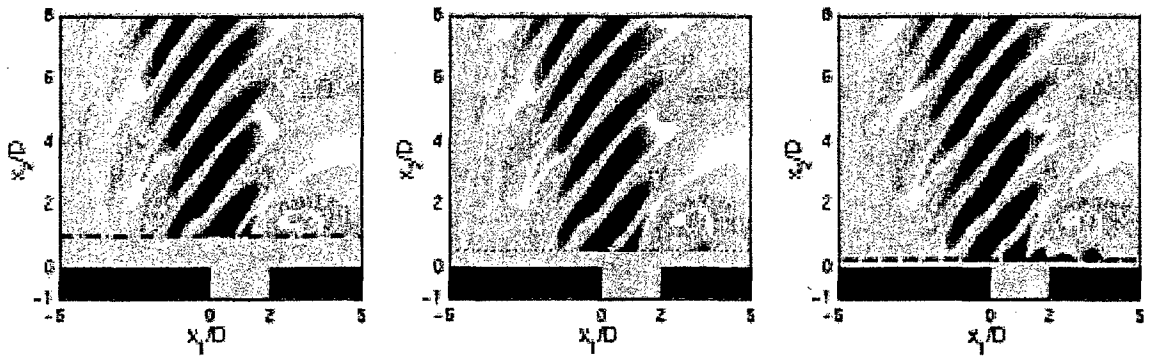

Figure 5: Pressure field calculated at the same time by a) FW-H WEM from L_1, b) FW-H WEM from L_2, c) FW-H WEM from L_3.

When we apply FW-H analogy, the surface integrals are evaluated on the physical rigid walls of the cavity and the volume integration is performed over the two surfaces S_1 and S_2 depicted in figure 3. The evaluation of volume integrals of T_{ij} are sensible to truncature effets, especially in the streamwise direction where the source terms decrease slowly. It is due to the presence of advected vortices, ejected from the cavity during the clipping process, in the reattached boundary layer on the downstream wall. By summing the volume and surface contributions (fig. 6a), we reconstruct the total sound field in reasonably good agreement with the DNS reference solution of figure 6b. A quantitative comparison with the other methods is provided by the pressure profiles and far-field directivity of figure 7. The results of the two WEM are similar and in fairly agreement with the DNS reference solution whereas more differences can be seen for the acoustic analogy profile. The main discrepancies for the directivity occur near the small angles θ (i.e. in the downstream direction) where the volume integration is abruptly cut by the end of the computational domain at $x_1 = 5D$, leading to truncature errors.

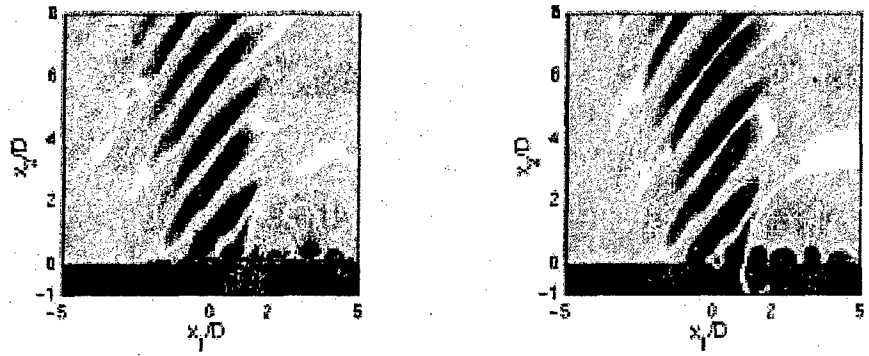

Figure 6: Pressure field calculated at the same time by a) FW-H analogy (surface + volume integrals), b) DNS reference solution.

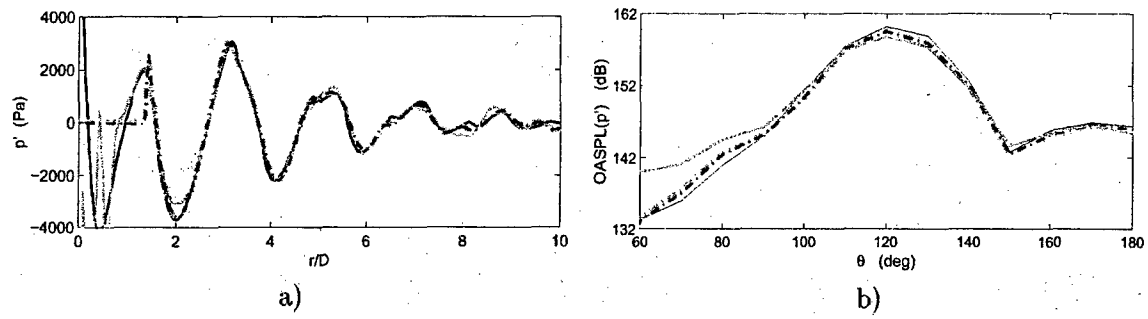

Figure 7: a), Pressure profile along the line $x_1 + x_2 = 2D$ ($r = \sqrt{x_1^2 + x_2^2}$) b), Overall sound pressure level as function of θ measured from streamwise axis with center at the downstream edge of the cavity. ($-\cdot-\cdot$) Kirchhoff's method from L_1, ($-\cdot-\cdot$) FW-H WEM from L_1, (——) FW-H analogy, (——) DNS.

However, FW-H analogy allows a better understanding of the structure of the radiated field than WEM since the direct and reflected sound field can be separated. Following reflection's theorem of Powell,[24] we can indeed argue that the volume integral (fig. 8a) represents the direct radiated field, and the surface integrals (fig. 8b) show essentially the reflected part of the field due to the cavity walls. These two fields at the same frequency give an interference figure where the two waves patterns are still distinguishable in our case because the cavity is not compact at the oscillation frequency ($L/\lambda = 0.47$).

The FW-H analogy provides more informations than the WEM but is more expensive in CPU time because of the evaluation of volume integral (surface integral in 2-D) whereas wave extrapolation methods need only surface integral (line integral in 2-D). For example, the computation time needed by the FW-H WEM is around 13 minutes, whereas the FW-H analogy requires 17 hours, on a Dec α computer. For the purpose of comparison, the DNS would take 320 hours on this machine.

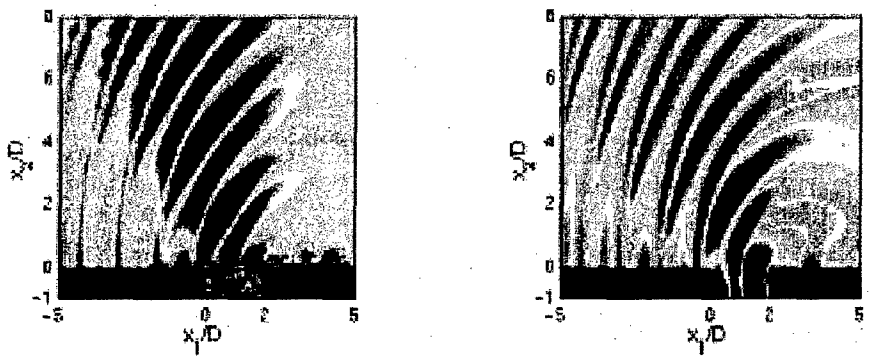

Figure 8: Pressure field obtained corresponding to: a) volume integral part of FW-H analogy, and b) surface integral part of FW-H analogy.

4. Conclusion

In a first part, a direct calculation of the sound radiated by a flow over a 2-D rectangular cavity is carried out. To this end, a DNS is performed using CAA numerical methods. This approach is expensive but is able to give all the interactions between flow and acoustic, and provides a powerful tool to determine noise generation mechanisms. The directly computed sound field is qualitatively and quantitatively consistent with Karamcheti's measurements in the same configuration.

The results of DNS are then successfully compared to three hybrid methods which use the DNS aerodynamic quantities to solve integral formulations. The wave extrapolation methods, like Kirchhoff's or porous FW-H methods, are relatively unaffected by the location of the control surface and constitute interesting complementary tools to extend CAA near-field to the far-field. Acoustic analogy is less efficient because volume integrations are costly and sensible to truncature effects. Nevertheless, it allows a separation between direct and reflected sound fields, which is useful for an analysis of radiation patterns.

To extend the present investigation, a 3-D simulation should be carried out. The recirculation zone inside the cavity is indeed characterized by a three-dimensional turbulent mixing, even if the development of the shear layer is almost two-dimensional. Such a study is under way.

Acknowledgments

Computing time is supplied by Institut du Développement et des Ressources en Informatique Scientifique (IDRIS - CNRS). The authors would like to thank Christophe Bogey for providing ALESIA code, and for many useful discussions and suggestions during the course of this work.

References

[1]ROCKWELL, D., 1983, Oscillations of impinging shear layers, *AIAA Journal*, **21**(5), p. 645–664.

[2]ROSSITER, J.E. Wind-tunnel experiments on the flow over rectangular cavities at subsonic and transonic speeds. Technical Report 3438, Aeronautical Research Council Reports and Memoranda, 1964.

[3]KARAMCHETI, K. Acoustic radiation from two-dimensional rectangular cutouts in aerodynamic surfaces. *Tech. Note* 3487, N.A.C.A., 1955.

[4]HANKEY, W.L. & SHANG, J.S., 1980, Analyses of pressure oscillations in an open cavity, *AIAA Journal*, **18**(8), p. 892–898.

[5]ZHANG, X., RONA, A. & LILLEY, G.M., 1995, Far-field noise radiation from an unsteady supersonic cavity, *AIAA Paper 95-040.*

[6]COLONIUS, T., BASU, A.J. & ROWLEY, C.W., 1999, Numerical investigation of the flow past a cavity, *AIAA Paper 99-1912.*

[7]SHIEH, C.M. & MORRIS, P.J., 1999, Parallel numerical simulation of subsonic cavity noise, *AIAA Paper 99-1891.*

[8]SHIEH, C.M. & MORRIS, P.J., 2000, Parallel computational aeroacoustic simulation of turbulent subsonic cavity flow, *AIAA Paper 2000-1914.*

[9]GLOERFELT, X., BAILLY, C. & JUVÉ, D., 2001, Computation of the noise radiated by a subsonic cavity using direct simulation and acoustic analogy, *AIAA Paper 2001-2226.*

[10]BOGEY, C., BAILLY, C. & JUVÉ, D., 2000, Numerical simulation of sound generated by vortex pairing in a mixing layer, *AIAA Journal*, **38**(12), p. 2210–2218.

[11]TAM, C.K.W. & DONG, Z., 1996, Radiation and outflow boundary conditions for direct computation of acoustic and flow disturbances in a nonuniform mean flow, *J. Comput. Acous.*, **4**(2), p. 175–201.

[12]BRENTNER, K.S., 2000, Modeling aerodynamically generated sound: Recent advances in rotor noise prediction, *AIAA Paper 2000-0345.*

[13]COLONIUS, T. & FREUND, J.B., 2000, Application of Lighthill equation to a Mach 1.92 turbulent jet, *AIAA Journal*, **38**(2), p. 368–370.

[14]BOGEY, C., BAILLY, C. & JUVÉ, D., 2001, Noise computation using Lighthill's equation with inclusion of mean flow - acoustics interactions, *AIAA Paper 2001-2255.*

[15]LIGHTHILL, M.J., 1952, On sound generated aerodynamically I. General theory, *Proc. of the Royal Society of London*, **A 211**, p. 564–587.

[16]FFOWCS WILLIAMS, J.E. & HAWKINGS, D.L., 1969, Sound generated by turbulence and surfaces in arbitrary motion, *Philosophical Transactions of the Royal Society*, **A264**(1151), p. 321–342.

[17]GOLDSTEIN, M.E., 1976, *Aeroacoustics*, McGraw-Hill, New York.

[18]LOCKARD, D.P., 2000, An efficient, two-dimensional implementation of the Ffowcs Williams and Hawkings equation, *J. Sound Vib.*, **229**(4), p. 897–911.

[19]DI FRANCESCANTONIO, P., 1997, A new boundary integral formulation for the prediction of sound radiation, *J. Sound Vib.*, **202**(4), p. 491–509.

[20]FARASSAT, F. & MYERS, M.K., 1988, Extension of Kirchhoff's formula to radiation from moving surfaces, *J. Sound Vib.*, **123**(3), p. 451–460.

[21]BRENTNER, K.S. & FARASSAT, F., 1998, An analytical comparison of the acoustic analogy and Kirchhoff formulation for moving surfaces, *AIAA Journal*, **36**(8), p. 1379–1386.

[22]SINGER, B.A., BRENTNER, K.S., LOCKARD, D.P. & LILLEY, G.M., 2000, Simulation of acoustic scattering from a trailing edge, *J. Sound Vib.*, **230**(3), p. 541–560.

[23]PRIEUR, J. & RAHIER, G., 1998, Comparison of Ffowcs Williams-Hawkings and Kirchhoff rotor noise calculations, *AIAA Paper 98-2376.*

[24]POWELL, A., 1960, Aerodynamic noise and the plane boundary, *J. Acoust. Soc. Am.*, **32**(8), p. 982–990.